ChemPubSoc Europe

DOI: 10.1002/open.201600066

Open Access ChemistryOPEN Full Papers

Ionic Liquid Solvation versus Catalysis: Computational Insight from a Multisubstituted Imidazole Synthesis in $[Et_2NH_2][HSO_4]$

Yusif Abdullayev,*[a, b] Vagif Abbasov,[b] Lucas C. Ducati,[c] Avtandil Talybov,[a, b] and Jochen Autschbach*[d]

The mechanisms of a tetrasubstituted imidazole [2-(2,4,5-triphenyl-1 H-imidazol-1-yl)ethan-1-ol] synthesis from benzil, benzaldehyde, ammonium acetate, and ethanolamine in $[Et_2NH_2][HSO_4]$ ionic liquid (IL) are studied computationally. The effects of the presence of the cationic and anionic components of the IL on transition states and intermediate structures, acting as a solvent versus as a catalyst, are determined. In IL-free medium, carbonyl hydroxylation when using a nucleophile (ammonia) proceeds with a Gibbs free energy ($\Delta G^{\neq}$) barrier of 49.4 kcal mol^{-1}. Cationic and anionic hydrogen-bond solute–solvent interactions with the IL decrease the barrier to 35.8 kcal mol^{-1}. $[Et_2NH_2][HSO_4]$ incorporation in the reaction changes the nature of the transition states and decreases the energy barriers dramatically, creating a catalytic effect. For example, carbonyl hydroxylation proceeds via two transition states, first proton donation to the carbonyl ($\Delta G^{\neq} = 9.2$ kcal mol^{-1}) from $[Et_2NH_2]^+$, and then deprotonation of ammonia ($\Delta G^{\neq} = 14.3$) via Et_2NH. Likewise, incorporation of the anion component $[HSO_4]^-$ of the IL gives comparable activation energies along the same reaction route and the lowest transition state for the product formation step. We propose a dual catalytic IL effect for the mechanism of imidazole formation. The computations demonstrate a clear distinction between IL solvent effects on the reaction and IL catalysis.

1. Introduction

Ionic liquids (ILs) have been widely applied in recent decades as solvents in organic synthesis, because of their availability, high efficiency, low cost, and 'green' aspects.[1] The dehydration reaction of fructose was catalyzed by acidic ILs immobilized on silica.[2] Simple Brønsted acidic ILs have been used as catalysts and media for efficient Fischer esterification. However, only the anion component of the IL is considered to take part in the esterification process. Various cationic components were tested with $[HSO_4]^-$ and the effectiveness of simple alkylammonium-containing ILs, compared to other bulky cations, was rationalized by their good solubility in water.[3] Wagh and Bhanage used a Brønsted-acidic IL in quantitative amounts in organic synthesis as an alternative to catalytic amounts of a precious-metal catalyst.[4]

It has recently been suggested in a joint experimental–computational study that an IL may be catalytically active.[5] However, in the mechanism described in the article, the IL stabilizes the transition states through electrostatic interactions and hydrogen bonding, which may alternatively be considered as solvation rather than catalysis. Herein, we would like to establish a clear distinction between the IL aiding a reaction as a solvent, as compared to acting as a catalyst.

Recently, experiments were performed using the reaction shown in Scheme 1 and the very simple IL in Scheme 2. The starting compounds and the IL were mixed together and the reaction proceeded at 100 °C in a one-pot synthesis. This type of synthetic procedure is known to be commercially viable and free of toxic intermediate release, and the desired product could be achieved safely. Remarkably, the reaction completed with 98% yield in only 20 min.[6] This is very surprising, because a similar $InCl_3 \cdot 3H_2O$-catalyzed reaction reaches only 84% conversion after 6 h.[7] The presence of $[Et_2NH_2][HSO_4]$ also improves the tetrasubstituted imidazole formation reaction considerably in terms of yield and reaction time, as compared to $Yb(OTf)_3$, $K_5CoW_{12}O_{40} \cdot 3H_2O$,[9] $NaHSO_4$/silica gel,[10] iodine,[11] and $Zr(acac)_4$.[12] $[Et_2NH_2][HSO_4]$ could catalyze the esterification (88% yield in 4 h) and tetrasubstituted imidazole formation re-

[a] Y. Abdullayev, A. Talybov
Department of Chemical Engineering, Qafqaz University
Hasan Aliyev Str. 120, Baku, Absheron AZ0101 (Azerbaijan)
E-mail: yabdullayev@qu.edu.az

[b] Y. Abdullayev, V. Abbasov, A. Talybov
Institute of Petrochemical Processes
Azerbaijan National Academy of Sciences, Baku AZ1025 (Azerbaijan)

[c] L. C. Ducati
Department of Fundamental Chemistry, Institute of Chemistry
University of São Paulo
Av. Prof. Lineu Prestes, 748, 05508-000 São Paulo (Brazil)

[d] J. Autschbach
Department of Chemistry, University at Buffalo
State University of New York, Buffalo, NY 14260-3000 (USA)
E-mail: jochena@buffalo.edu

Supporting Information for this article can be found under http://dx.doi.org/10.1002/open.201600066.

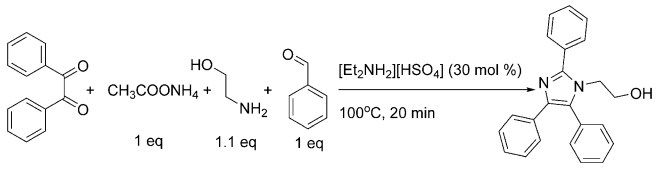

Scheme 1. The reaction considered in this study.

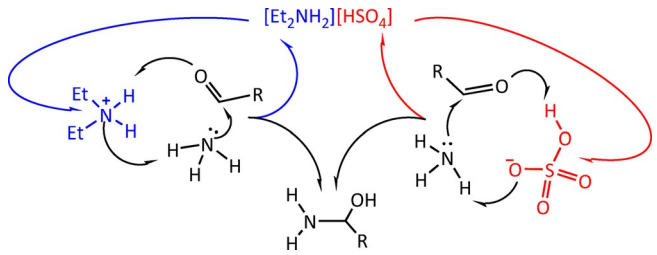

Scheme 2. Cationic and anionic components of IL dual catalytic effect on nucleophilic addition.

actions. Changing protic $[HSO_4]^-$ to an aprotic anion such as $[BF_4]^-$ causes the yield of esterification to decrease to 50% and acid needs to be supplemented to the medium to increase the yield.[3] These known findings cause us to question whether the IL is indeed acting as a catalyst. Moreover, why does the replacement of $[HSO_4]^-$ yield such a significant reduction in conversion?

Computational chemistry has become a prime tool for detailed studies of reaction mechanisms and catalysis.[13] Herein, we provide answers to the above questions from a detail mechanistic computational approach at the Kohn–Sham (KS) density functional theory (DFT) level. The imidazole formation reaction of Scheme 1 is used as an example because of the very efficient conversion in the presence of the IL. We chose benzaldehyde among the array of aldehydes that were used in our experimental work,[6] because of its simple structure, along with other reagents, namely benzil, ethanolamine, ammonium acetate, and [Et_2NH_2][HSO_4], to conduct theoretical calculations on the reaction. The one-pot synthesis of substituted imidazoles is also a suitable example, representing more general nucleophilic addition and cyclocondensation reactions.[14] Moreover, multicomponent imidazoles are important structural motifs for antimycobacterial agents in the treatment of tuberculosis,[15] in peptidomimetics design,[16] as antifungal agents,[17] and they are also found in DNA.[18] Imidazole scaffolds are also utilized as anticancer agents,[19] corrosion inhibitors[20] and catholytes for hybrid Li–air batteries.[21] Our main goal in this work is to elucidate the IL catalytic effect and illustrate the distinction between IL solvation versus catalytic effects.

Brønsted-acidic ILs are perfect agents for proton exchange (see Scheme 2) in a nucleophilic addition reaction. $[HSO_4]^-$ may act as a proton donor and it has been hypothesized in a recent study that it may also act as a proton acceptor as the anionic component of 2-ethyl imidazolium hydrogen sulfate.[22] $[HSO_4]^-$, as the acidic component of the IL, can donate a proton to the carbonyl-containing species rather easily to become $[SO_4]^{2-}$, which may then accept a proton from a nucleophile (ammonia or benzyl amine in this study) and convert back to hydrosulfate. Strong acids, such as H_2SO_4, are not capable of acting in the same way. In the H_2SO_4 case, there is a low concentration of proton acceptors in the medium to catalyze the reaction as well as the IL. The cationic component of the IL, $[Et_2NH_2]^+$, can act in a similar way in the reaction of Scheme 1, for example, by donating a proton to carbonyl, becoming a strong base, and easily abstracting a proton from the ammonia interacting with the electropositive carbon. Our computations reveal that the anionic and the cationic component of the IL together cause a *dual effect* when catalyzing the multisubstituted imidazole synthesis reaction. The effects from the IL acting as a solvent are also investigated and described.

Computational Details

The computations were performed by using Kohn–Sham DFT with the M06L functional[23] and 6-31G*[24] basis sets for H, C, N, and O. The 6-31++G(d,p) basis was used for sulfur in the IL, according to recent recommendations.[25] The Gaussian 09 package was used for all calculations.[26] At this level of theory, the optimized and the experimentally determined X-ray structure of the reaction product are in good agreement (Table S1 and Figure S1 in the Supporting Information). The structures of the starting materials, intermediates, and transition-state structures were optimized in gas phase and with a solvent module without symmetry constraints. Solvent effects were incorporated by using an SMD solvation model (Figure S3) for acetic acid ($\varepsilon = 6.2528$).[27] Single-point energies of all stationary structures (Figure S4) were evaluated by using the same basis used for the structure optimizations, and with the 6-31++G(d,p) basis for all atoms. The Gibbs free energy corrections from the smaller basis set calculations were combined with the single-point energies calculated with the larger basis to arrive at the free energies for all starting materials, stationary structures, intermediates, and products. We note that the reaction barriers do not change considerably upon switching to the larger basis for the single-point energies. The reaction path was calculated both for ambient conditions (1 atm, 298.15 K) and for 100 °C (1 atm, 373 K). Optimized Cartesian coordinates, total energies, Gibbs energies, and enthalpies of all structures are provided in the Supporting Information.

Under the reaction conditions, ammonium acetate is decomposed and ammonia reacts directly with carbonyl species (benzil, benzaldehyde). Nucleophiles and carbonyl-containing species in these one-pot conditions imply four possible interactions for the starting point of the reaction: ammonia + benzaldehyde, ammonia + benzil, ETA + benzaldehyde, and ETA + benzil. Hence, ammonia coming from ammonium acetate is only thought to be present as a nucleophile and acetic acid may act as a solvent. We calculated the reaction steps twice, first in the gas phase and then with a solvent model for AcOH, starting with the ETA + benzil interaction (see the Supporting Information). Based on the energy barriers, AcOH as a solvent is not a deciding factor in rendering the reaction more feasible. Moreover, in the gas phase, this route turned out to afford high-energy barriers compared to the route that starts with an ammonia + benzaldehyde interaction. Hence, we decided to proceed with the ammonia + benzaldeyde interaction as a starting point to identify IL effects on the whole reaction profile. Both molecules are relatively small and the probability of reactive collisions

among them was deemed more likely compared to the other starting possibilities. Moreover, the reaction route starting with the ETA + benzaldehyde interaction is the same as the calculated ammonia + benzaldehyde route after the diamine formation: ETA and benzaldehyde form amino(phenyl)methanol, and then water extrusion yields an imine moiety [2-(benzylideneamino)ethan-1-ol]. Further reaction with ammonia creates a geminal diamine intermediate that is the same as the intermediate **F_INT5** or **S_INT5** discussed below in the reaction starting with the ammonia + benzaldehyde interaction. The route starting with the ammonia + benzil interaction becomes the same as the calculated ETA + benzil interaction route after the third step (see Figure S3). **INT5** of Figure S5 is the first common intermediate for these two routes, and further intermediates and transition states corresponds to this route. For the above reasons, the reaction path discussed in the following is the one starting with the ammonia + benzaldehyde interaction.

2. Results and Discussion

The reaction steps were calculated in three different ways to obtain reaction profiles free of interactions with the IL, with IL solvation, and with the IL being catalytically active.

2.1. IL-Free Route (F)

The imidazole formation reaction profile calculated in the gas phase, without IL interactions, is summarized in Figure 1. The potential energy surface (PES) presented by the reaction profile illustrates that the imidazole formation reaction is conceivable through hydroxylation and dehydration steps. **F_INT2** is the intermediate product of ammonia reacting with benzaldehyde, and can be formed through the **F_TS1** transition state at 49.4 kcal mol^{-1} above the starting materials. Proton transfer to hydroxyl makes **F_INT2** conversion to **F_INT3** (imine) possible; this is the dehydration step via **F_TS2** with a 44.4 kcal mol^{-1} barrier and results in water abstraction. **F_INT3** reaction with ETA is calculated to have a high barrier (54.0 kcal mol^{-1}) and yields a geminal diamine intermediate (**F_INT5**). The next step is benzil addition to **F_INT5**; it has a similar barrier to the diamine formation step and yields 33.0 kcal mol^{-1} endergonic **F_INT7**. The following ring closure goes along with a proton transfer to the carbonyl oxygen; its barrier is calculated to be 42.7 kcal mol^{-1}. Further dehydration and deprotonation steps lead to the formation of the aromatic tetrasubstituted imidazole product (**F_PROD**). Both **F_TS6** and **F_TS7** are transition states leading to dehydration. Interestingly, **F_TS6** is 12.6 kcal higher in energy than **F_TS7** despite the proton transfer in **F_TS7** taking place over a long (1.65 Å) distance over two bonds (Ph–C–N–C–Ph). The overall reaction is 1.3 kcal mol^{-1} exergonic at 373 K. For comparison, the relative Gibbs free energies (ΔG_{298}) at 298 K are also shown in Figure 1. Formation of all intermediates and the final product is about the same in terms of Gibbs free energy at 298 and 373 K, which indicates that high temperature is not vital for the multisubstituted imidazole synthesis.

2.2. IL Solvation (S)

To investigate solvent–solute-type interactions between the IL and the various species occurring in the reaction, one each of the cationic and anionic components of the IL were added into the optimizations of all intermediates and transition states involved in the reaction profile. In particular, IL components were placed near to bond-breaking and bond-formation sites of transition-state structures (we refer to these as 'active sites'

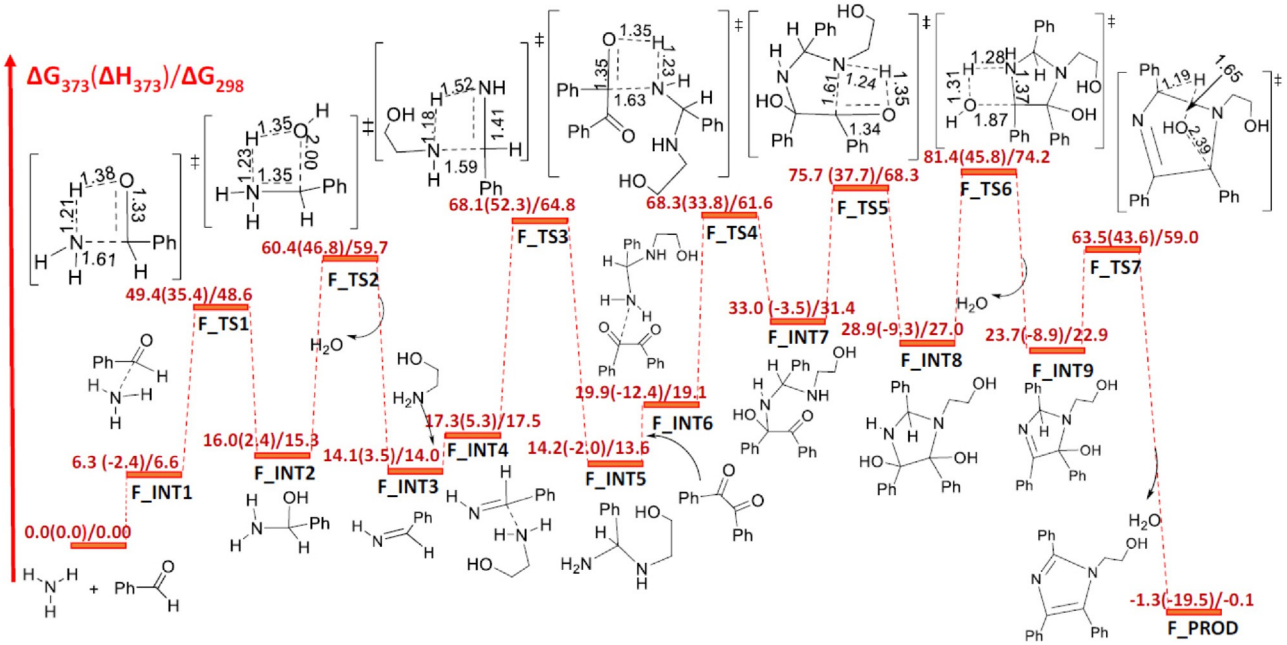

Figure 1. PES is designed for the reaction given in Scheme 1 without the IL (IL-free, **F**) in the gas phase at 1 atm and 373 K. For comparison, the free energies at 298 K are also included. Gibbs free energies and enthalpies are relative to reactants + IL + ETA + benzil. Important bond lengths given in Å.

in the following). This is generally effective, because the IL components tend to interact with an active site of a transition state through electrostatic- and hydrogen-bonding-type interactions. For intermediates, we let the IRC (intrinsic reaction coordinate) search determine the placement of the IL components. The concentration of the IL (30 mol% in the experiment) is not high, and we can assume that, on average, not more than one IL ion pair is interacting with the transition states and intermediates. Owing to the strong coulombic attraction, the cationic and anionic components of the IL remain in spatial proximity in the optimized structures. For the sake of clarity, we emphasize only the closest interactions in Figure 2, that is, in some cases the cationic or anionic component of the IL is not shown.

The first amino(phenyl)methanol formation step **S_INT2** proceeds through **S_TS1**; the latter is found to be 35.8 kcal mol^{-1} above the starting materials. The interaction with the IL causes the formation of a hydrogen-bond network, which is responsible for decreasing the energy barrier of this step by 13.6 kcal compared to the **F** route (Figure 2 vs. Figure 1). The PES illustrates closer and more effective cationic and anionic interaction distances in the transition states. For example, the $[Et_2NH_2]^+$ interaction (1.62 Å) with the carbonyl oxygen causes the C=O bond to elongate from 1.33 Å in **F_TS1** to 1.39 Å in **S_TS1**. The C=O elongation promotes proton transfer from ammonia and also causes stretching of the N–H bond to 1.26 Å. The same effect can be observed for the following hydroxylation and dehydration steps along the reaction path. **S_INT2** is amino(phenyl)methanol and is converted to **S_INT3** via **S_TS2** with a 39.7 kcal mol^{-1} energy barrier. The nucleophilic amine (ETA) attacks imine **S_INT3** bearing a partially positive sp^2 carbon. Adding ETA to **S_INT3** results in the formation of **S_INT5** (geminal diamine), which is calculated to afford a 36.6 kcal mol^{-1} barrier; this is 17.4 kcal lower than that for the **F** case. The anionic component $[HSO_4]^-$ of the IL is as important as the cationic component for decreasing energy barriers. For instance, it can be seen in Figure 2 that $[HSO_4]^-$ forms hydrogen bonds with **S_TS5**, **S_TS6** and **S_TS7**. In **S_TS5**, $[HSO_4]^-$ interacts with hydroxyl at a distance of 1.76 Å, which causes the energy barrier to decrease by 9 kcal compared to the **F** path. In the next transition state, the $[HSO_4]^-$ proton interacts with nitrogen (1.83 Å); this is one of the four active sites of the **S_TS6** transition state structure. A partially negative oxygen of $[HSO_4]^-$ forms another interaction with the hydroxyl group on the imidazole ring (1.82 Å). These interactions very effectively bring down the energy barrier by 18 kcal mol^{-1}. In **S_TS7**, $[HSO_4]^-$ interacts with nitrogen at a distance of 1.95 Å, but not with one of the four active sites of the transition state. Nonetheless, the interaction with the IL changes the distances between the transition-state active sites relative to **F_TS7** in Figure 1, and the energy barrier is 12.2 kcal lower than the **F** path.

Clearly, the IL can significantly affect the energetics of the reaction, even if it is mainly thought of as a solvent. As described in more detail below, the IRC connects the final transition state to a less effective solvated product (**S_PROD***). After adjustment to the more effectively solvated product, ΔG of the **S** profile is −13.9 kcal mol^{-1}. Therefore, the **S** reaction profile is 12.6 kcal more exergonic than the **F** route (Figure 2). More importantly, in the absence of IL, the desired product formation goes through a 9.5 kcal higher barrier for the benzil addition (**F_INT5**→**F_INT7**), and the water-elimination step (**F_INT8**→**F_INT9**) is 18 kcal higher. Despite the energy barriers being lower with IL solvation, in comparison to the **F** route, these interactions are not highly effective, because the IL is not fundamentally altering the mechanism and not acting differently from a strongly polar solvent capable of hydrogen bonding. Therefore, we continue to explore the reaction with the aim of identifying a more genuine IL catalytic effect.

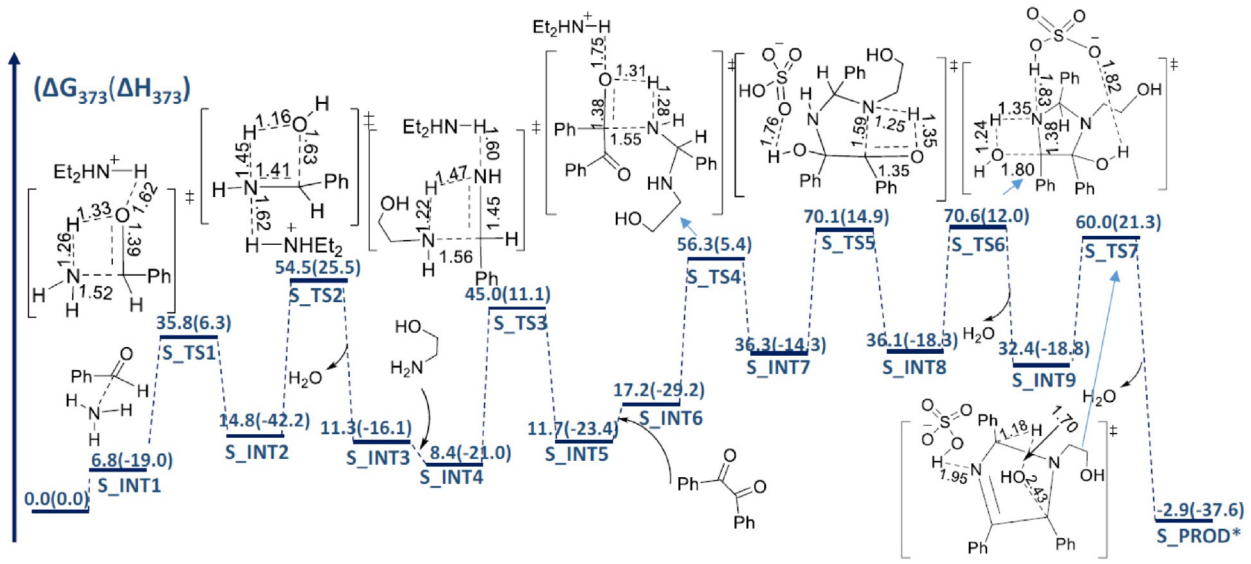

Figure 2. PES is designed for the reaction involving interaction with one $[Et_2NH_2][HSO_4]$ ion pair in order to see the IL solvation effect (IL-solvation, **S**) in the gas phase at 1 atm and 373 K. Gibbs free energies and enthalpies are calculated relative to reactants + IL + ETA + benzil. Important bond lengths are given in Å. For clarity, intermediate structures are omitted. They can be found in Figure 1.

2.3. IL Catalysis (C)

We tested the amino(phenyl)methanol formation path of Figure 2, but now allowing for proton transfer between the IL and other species present. Remarkably, proton transfer between the IL and carbonyl or amine functional groups in the transition states strongly lowers the energy barriers compared to the IL solvation route. The amino(phenyl)methanol formation path was calculated twice, with $[Et_2NH_2]^+$ and $[HSO_4]^-$ incorporation, respectively. The IL catalytic effect takes place through proton exchange between the cationic and anionic components of the IL and carbonyl, amine, and hydroxyl functional groups, which is evidently different from the IL solvation effect.

2.3.1. $[Et_2NH_2]^+$ Incorporation

Figure 3 compares the **F**, **S**, and IL cation catalysis (**CC**) variants of amino(phenyl)methanol formation. This reaction step would require an activation energy of 49.4 kcal mol^{-1} in the **F** route and 35.8 kcal mol^{-1} in the **S** route. In the **CC** route, $[Et_2NH_2]^+$ readily shares a proton with the carbonyl oxygen. The corresponding transition state is **CC_TS1** and is calculated to be only 9.2 kcal mol^{-1} higher in energy than the starting materials. The subsequent deprotonation of ammonia to reach the amino(phenyl)methanol intermediate product has an even smaller barrier of 6.4 kcal mol^{-1} (**CC_TS2**) relative to the intermediate.

Figure 4 continues the comparison of the **S** and **CC** routes. The main difference between them is that **CC_INT4** is the imine cation [natural bond orbital (NBO) analysis clearly indicates the presence of a localized C=N double bond] stabilized by the polar environment, whereas **S_INT3** is a neutral imine intermediate. The latter is lower in energy, but its formation has a higher barrier. Further addition of ETA following the **S** path also affords a considerably higher barrier. In the catalytic route to diamine formation (**S_INT5**), the hydroxylation and dehydration steps afford higher barriers than the deprotonation steps and can be considered as rate determining up to this point in the reaction.

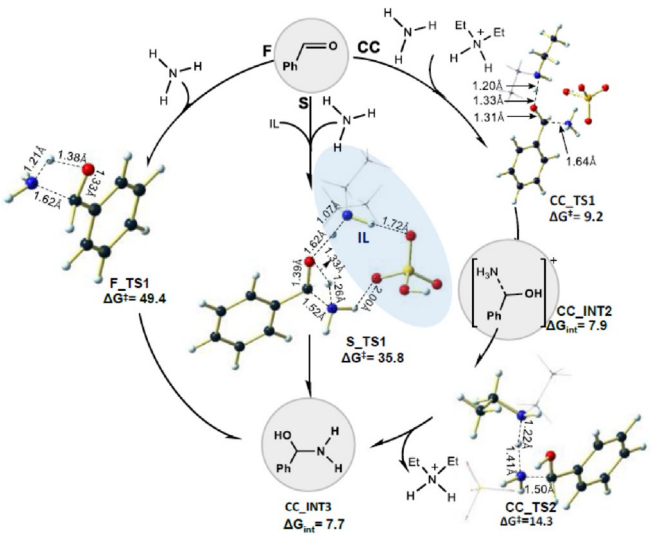

Figure 3. Calculated mechanisms for the amino(phenyl)methanol formation step. **F**: IL-free route. **S**: IL solvation route. **CC**: ($[Et_2NH_2]^+$) catalytic route. Transition-state ($\Delta G^{\ddagger}$) and intermediate (ΔG_{int}) Gibbs free energies and the optimized structures of the transition states structures with important bond lengths are added to the figure.

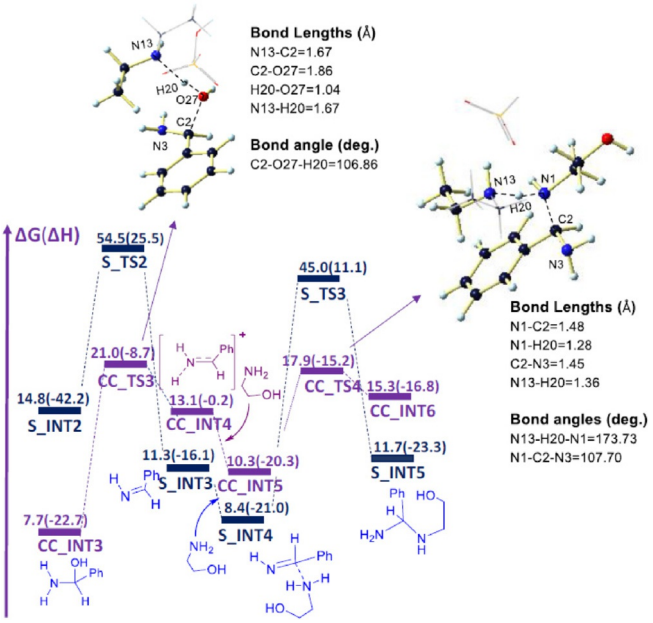

Figure 4. The diamine formation step based on the incorporation of the IL cation in the transition states (purple). For comparison, the IL solvation path (dark blue) is included in the figure. In the **C_TS3** and **C_TS4** structures, the Et groups of $[Et_2NH_2]^+$ and $[HSO_4]^-$ are omitted for the sake of clarity.

What renders the **CC** route more feasible? For instance, the **CC** transition states in the amino(phenyl)methanol formation step are overall different from the **F** and **S** routes, because of the separate hydroxylation and deprotonation steps, which evidently require less activation energy overall. To see why, we turn to the optimized transition-state structures in Figures 3 and 4 to scrutinize the bond distances. In Figure 3, the **F_TS1**, **S_TS1**, and **CC_TS1** structures exhibit important differences. In the **F** and **S** routes, the benzaldehyde carbonyl bond elongates more compared to the **CC** transition states, which is, for the most part, associated with an energetic penalty. The optimized benzaldehyde carbonyl bond distance is 1.22 Å. In **F_TS1**, the carbonyl bond is stretched to 1.33 Å, and even further in **S_TS1** (1.39 Å), which is assisted by a balancing stabilization from the hydrogen-bonding network. In **CC_TS1**, the corresponding distance is 1.31 Å (Figure 3). The IL cation transfers the proton to the carbonyl oxygen without elongating the carbonyl double bond too much. The follow-up transfer of a proton back to the IL is accomplished with little of a barrier.

2.3.2. $[HSO_4]^-$ Incorporation

The anionic catalytic (**CA**) effect is shown in Figure 5. The proton-exchange steps in the **CC** path inspired us to test the anionic component $[HSO_4]^-$ for the same mechanism, because of its acidic nature. The diamine formation step was recalculated with incorporation of the IL anionic component into the

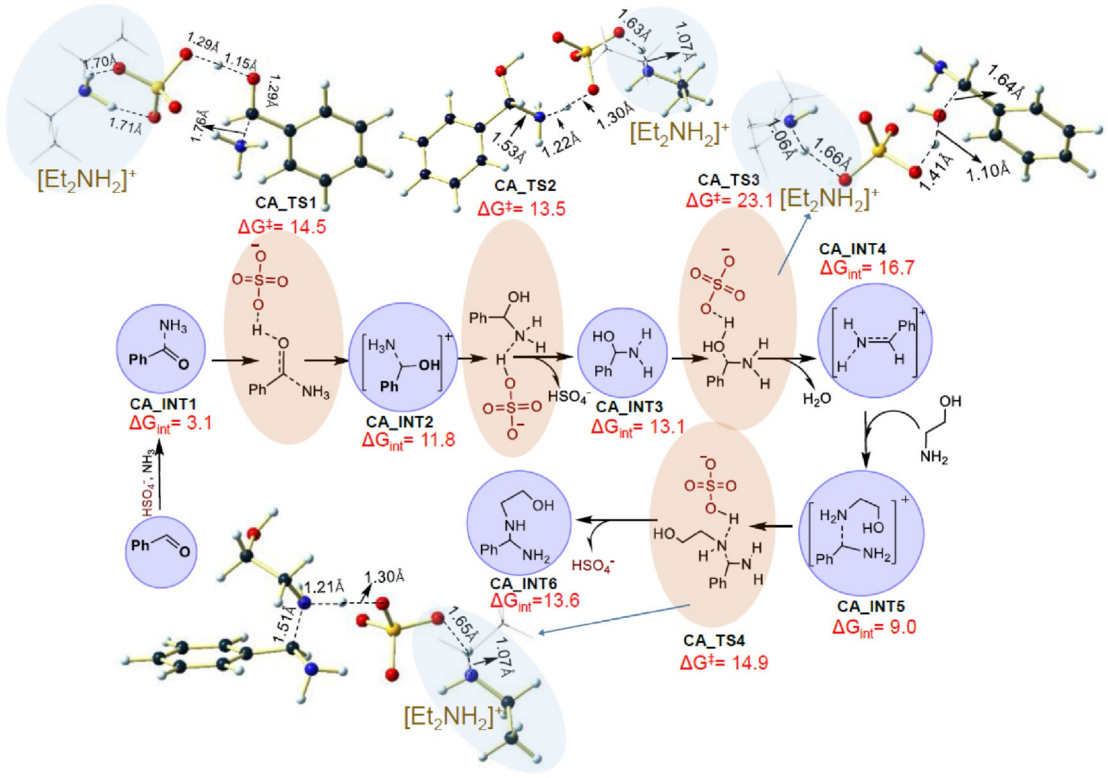

Figure 5. Calculated mechanism for the diamine formation step with the IL anion $[HSO_4]^-$ (**CA**) catalytic effect. The optimized structures of the transition states with important bond lengths are added to the figure. The Et groups of $[Et_2NH_2]^+$ are omitted for clarity.

transition-state structures. Figure 5 illustrates that $[HSO_4]^-$ does in fact act quite similar to the IL cationic component. The hydroxylation transition-state (**CA_TS1**) barrier is found to be 14.5 kcal mol^{-1}, which is 5.3 kcal higher than in the **CC** route. The ammonia deprotonation (**CA_TS2**) barrier is 1.7 kcal mol^{-1}, which is 4.7 kcal less than for **CC**. The following dehydration barrier (**CA_TS3**) is 10 kcal mol^{-1}, that is, 3.3 kcal less than in the **CC** route. The ETA addition transition state (**CA_TS4**) represents a 5.9 kcal barrier and results in diamine formation.

Overall, with reaction steps that involve a protonation–deprotonation water-abstraction sequence, the **CA** and **CC** routes offer similarly effective catalysis. We, therefore, decided not to calculate similar sequences later in the reaction along both routes, but only along the **CA** path. Another reason for focusing on **CA** is that **CC** affords a much higher transition state in a C–H deprotonation step (vide infra, proton **d** abstraction in Scheme 3). A major difference between the **CC** and the **CA** routes is that, in the former, the cationic IL component acts effectively as a catalyst mostly by itself. On the contrary, in the **CA** route, the anionic and cationic components must act together in order to facilitate a significant decrease in the energy barriers compared to the solvation route. It can be seen from the Figure 5 transition states that $[HSO_4]^-$ is the catalytically active component of the IL, but $[Et_2NH_2]^+$ is interacting with the anionic component at relatively close distances through one or two hydrogen bonds. For example, in **CA_TS1**, both $[Et_2NH_2]^+$ protons are interacting with the $[HSO_4]^-$ oxygens at a distance of about 1.70 Å. In **CA_TS2**, one of the $[Et_2NH_2]^+$ protons interacts with the IL (1.63 Å; this effect is highlighted in sky blue color in Figure 5). In general, throughout the **CA** path, $[Et_2NH_2]^+$ interacts with the anionic component at around 1.62–1.71 Å, and facilitates the IL anion binding in specific orientations to transfer a proton. This effect is illustrated in Figure 5, and confirmed once more on the imidazole formation step. Further support of the role of $[Et_2NH_2]^+$ in the **CA** route is provided by the fact that, in its absence, some of the transition states could not be located, despite many attempts. An example is **CA_TS4**. In contrast, in the **CC** route transition-state structures (Figures 3 and 4), in most cases, $[HSO_4]^-$ is more than 2.0 Å away from the cation protons.

Until the formation of the diamine intermediate (**CC_INT6**, **CA_INT6**), the hydroxylation and dehydration steps are rate determining in both the **CA** and the **CC** routes. We expected that the **CA** would be a viable alternative to **CC** in the following steps as well, and calculated the remainder of the reaction path with $[HSO_4]^-$ incorporation. The steps **S_INT5**→**S_INT8** in the IL solvation route were examined for the **CA** effect; the re-

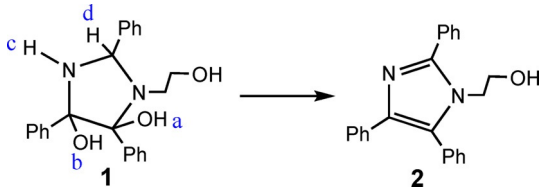

Scheme 3. The tetrasubstituted imidazole formation path.

sults are shown in the Supporting Information as the **CA_INT6→CA_INT11** transition (Figure S5). The tetrasubstituted imidazole product formation (Scheme 3) step (**S_INT8→S_PROD***) of Figure 2 was recalculated as the **CA_INT11→CA_PROD** transformation (Figure 6). In the **S** route, the dehydration process is the proton **c** transfer to hydroxyl **b** with a 34.5 kcal mol^{-1} (**S_TS6**) barrier. The further dehydration step is proton **d** migration over two bonds to hydroxyl **a**, which affords an activation energy of 27.6 kcal mol^{-1} and yields the final product **2**. The **CA** process goes through step-by-step removal of substituents **a**, **b**, **c**, and **d** of intermediate **1** (corresponding to **S_INT8** in Figure 2 and **CA_INT11** in Figure 6) and requires four separate transition states. It is much more feasible than the **S** route. Hydroxyl **a** removal with $[HSO_4]^-$ incorporation is possible via transition state **CA_TS9**, representing a 11.2 kcal mol^{-1} energy barrier. The optimum conditions for the proton migration are C5–O6 bond elongation to 1.75 Å for hydroxyl **a**, and $[HSO_4]^-$ H10–O9 bond stretching up to 1.44 Å in the **CA_TS9** structure in Figure 6. The removal of proton **d** from C2 requires an activation energy of 5.7 kcal mol^{-1} via **CA_TS10**. For comparison, the corresponding **CC** barrier (**CC_TS10**) for the removal of proton **d** is 53.7 kcal mol^{-1}, which is not feasible compared to the **CA** route (see the Supporting Information for the optimized **CC_TS10** structure). The C2–H21 bond is elongated to 1.58 Å for migration to the sulfate ion in **CA_TS10**. Removal of hydroxyl **b** is possible via **CA_TS11** with a 3.5 kcal mol^{-1} barrier. Interestingly, removing hydroxyl **b** results in **CA_INT14** formation, which is 32 kcal mol^{-1} exergonic. Probably, partial π conjugation of the C–N–C bonds is responsible for rendering **CA_INT14** particularly stable. The corresponding **S_INT8→S_INT9** transformation (dehydration of hydroxyl **b** with proton **c** in one transition state, **S_TS6**) is only 3.7 kcal exergonic. Removal of proton **c** on **CA_INT14** is almost barrier free and renders the structure fully aromatic. **CA_INT14** conversion to the final product (**CA_PROD**) proceeds with a 1.4 kcal mol^{-1} barrier via **CA_TS12**. The reason for the very small energy barrier is related to a hydrogen-bond interaction between H24 of the $-(CH_2)_2-OH$ group and the sulfate O11 at a 1.77 Å distance.

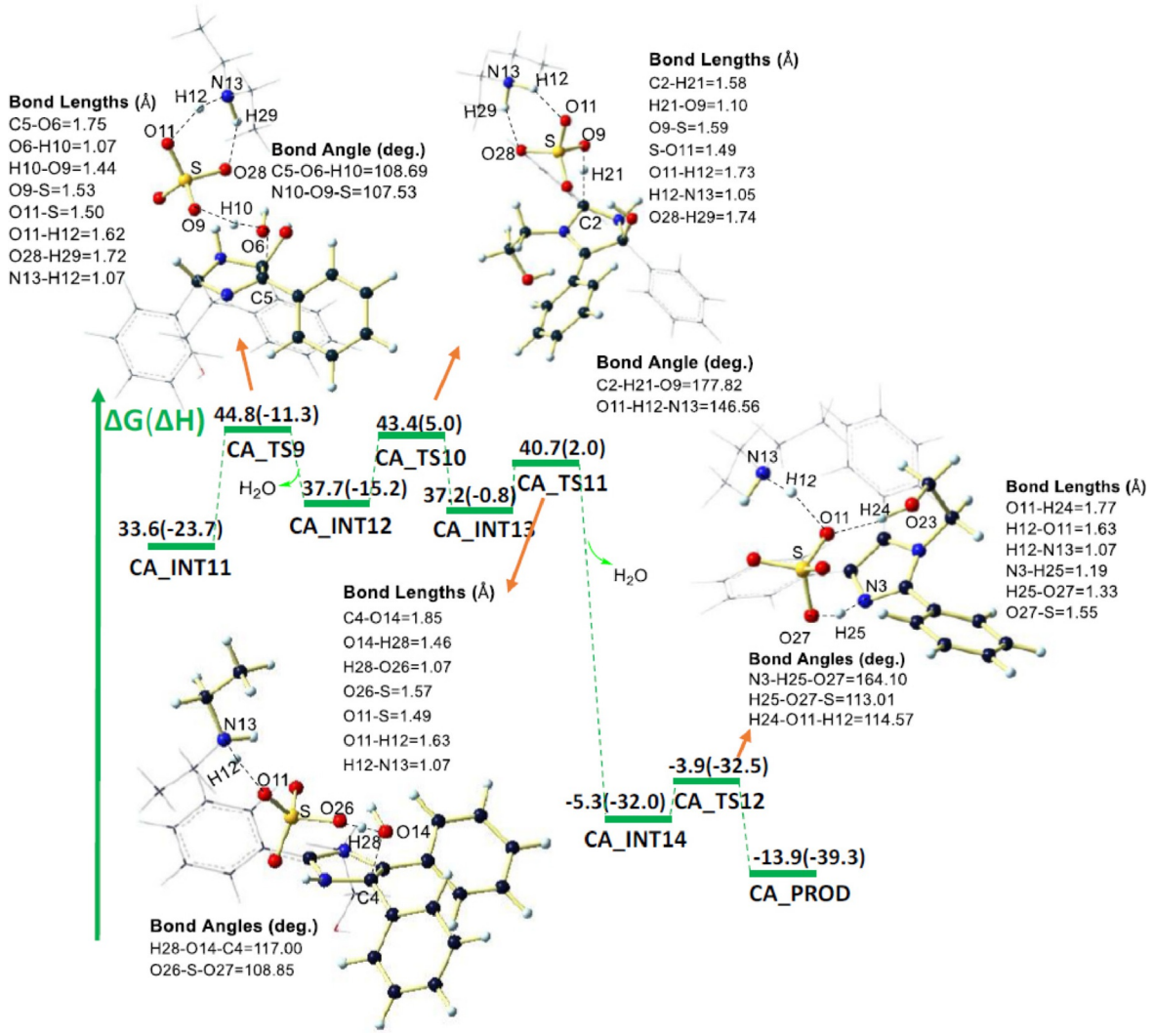

Figure 6. The imidazole-formation step with the IL anion $[HSO_4]^-$ catalytic effect. Transition states optimized structures with important bond lengths and angles are added to the figure. In the transition-state structures, Ph, Et, and $HO-(CH_2)_2-$ groups are omitted for the sake of clarity.

The **CC** and **CA** reaction paths are thermodynamically favorable over the **F** route and lead to a comparatively flat energy profile by decreasing the barriers. The increase of the ΔG magnitude in the presence of the IL is attributed to differential solvation of the reactants/product. In the solvent-only route, the product **S_PROD*** that is formed from the final transition state (**S_TS7**) as a result of the IRC search is less effectively solvated than **CA_PROD**, where the IL anionic component stabilizes the structure through two hydrogen bonds. Therefore, **S_PROD*** will convert to **CA_PROD** as the final product for both the **S** and **CA** routes, and ΔG is the same as for the catalytic routes, as it should be.

Overall, the calculations show that the reaction can yield the desired product with an IL *dual* (i.e. cationic and anionic) catalytic effect with much lower activation energies than can be achieved if the IL acts only as a solvent. Our calculations, therefore, rationalize the experimental observations that we reported previously[6] and answer the question "Why is the reaction completed in a very short time with a remarkably high yield?".

2.3.3. Kinetic Approach

To describe the efficiency of the catalytic route, the complete **S** and **CA** free-energy profiles are compared in Figure 7. The energetic span approximation (δG, here in terms of the Gibbs energy) is applied to illustrate the kinetic feasibility of the catalytic cycle [Eqs. (1) and (2)].[28]

$$TOF = \frac{k_B T}{h} e^{-\delta G/RT} \quad (1)$$

$$\delta G = \begin{cases} G_{TDTS} - G_{TDI} \text{ if TDTS appears after TDI} \\ G_{TDTS} - G_{TDI} + \Delta G_r \text{ if TDTS appears before TDI} \end{cases} \quad (2)$$

Here, *TOF* is the turnover frequency of the catalytic cycle, TDTS is the *TOF*-determining transition state, and TDI is the *TOF*-determining intermediate. TDTS is defined as the highest-energy transition state and the TDI is defined as the lowest-energy intermediate. ΔG_r is the reaction free energy. According to Ref. [28], when there are competing reaction paths with the same starting materials and products, as is the case here, the TDI is the lowest intermediate overall and the TDTS is the more favorable one among the pathways. Hence, **CA_TS9** is the TDTS and **S_INT4** of the solvation route is the TDI (the **CA** route produces this intermediate as a higher energy conformer). If the catalytic path is not available, **S_TS6** would be the TDTS. The δG value is 36.4 kcal mol^{-1} with both catalysis and solvation, whereas it is 62.2 kcal mol^{-1} with solvation only. Clearly, the IL catalysis leads to a dramatically increased turnover at 373 K [Eq. (3)]:

$$\frac{TOF_{IL-catalytic}}{TOF_{IL-solvation}} = 10^{15} \quad (3)$$

Owing to the sensitivity of the numerical result to small differences in δG, the actual *TOF* increase may be quite different. But, even if the power of 10 is smaller by several units, this would still lead to a dramatic increase in the efficiency of the reaction, owing to the IL catalysis versus solvation, which is our main point.

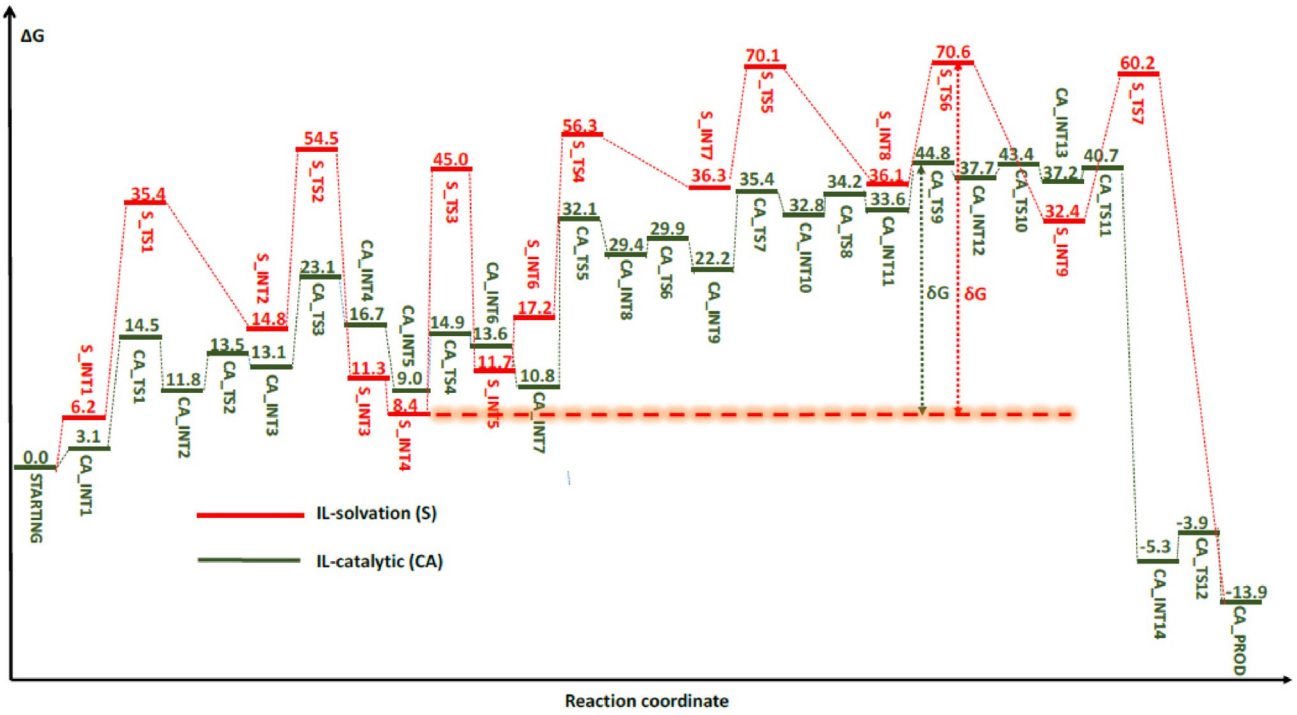

Figure 7. IL catalytic (**CA**) free-energy profile (green). IL solvation (**S**) free-energy profile (red).

3. Conclusions

Although IL solvation already leads to a significant lowering of the reaction barriers, the computations show that there are even more effective pathways, in which the IL acts as a catalyst through proton transfers. Brønsted-acidic ILs represent a good alternative to a strong acid for the catalysis of nucleophilic addition reactions. We computationally identified that the IL is a better catalyst than sulfuric acid and other metallic catalysts (Lewis acids). This study shows that $[Et_2NH_2][HSO_4]$ as a Brønsted-acidic IL is not simply a polar medium for the reaction. Especially with hydrosulfate as the anionic component of the IL, it acts as a proton-exchanging agent similar to the cation component of the IL. The tetrasubstituted imidazole formation reaction was calculated under IL-free, IL-solvation, and IL-catalytic conditions. The tetrasubstituted imidazole formation proceeds via intramolecular hydroxylation and deprotonation in the absence of the IL, but the reaction profile affords high barriers. In IL-catalytic case, the reaction mechanism is altered and the barriers are lowered, and this enables the reaction to proceed as experimentally observed. In the presence of the IL, the calculations indicate a number of different interactions:

1) IL solvation effect (**S**): The IL cationic and anionic components interact with the transition states and, in particular, significantly decrease the overall barriers. This is explained through the formation of a moderately strong hydrogen-bond network.
2) IL catalytic effect [cationic component (**CC**)]: $[Et_2NH_2]^+$ donates a proton for the hydroxylation of carbonyl (**CC_TS1**) and the dehydration of hydroxyl (**CC_TS3**). The opposite effect can be seen when a deprotonated Et_2NH cation (as a strong base) is incorporated into the transition states as a proton acceptor (**CC_TS2** and **CC_TS4**). The rate-determining energy barriers are those based on proton donation. The cases where $[Et_2NH_2]^+$ acts as a proton acceptor have significantly lower activation energies.
3) IL catalytic effect [anionic component (**CA**)]: $[HSO_4]^-$ also acts as a catalyst for the reaction. Moreover, the IL cationic component is interacting with the anionic component when the latter is catalytically active. Optimum interaction distances have been calculated at 1.63–1.71 Å for the cation proton and the anion oxygen. This interaction strongly facilitates the catalytic activity of the anionic IL component for proton exchange. In contrast, no such 'assistance' is required when the cationic component is catalytically active.
4) We have taken the opportunity to perform structural analysis of the product, which was not performed in our previous experimental study.[6] Details can be found in the Supporting Information. 2-(2,4,5-Triphenyl-1H-imidazol-1-yl)ethan-1-ol is more stable in the *gauche* conformer. Calculated proton NMR ^3J coupling constants and chemical shifts match well with experimental NMR data for this conformer.

The computations give detailed mechanistic insight into the $[Et_2NH_2][HSO_4]$ IL catalytic effect. Hydrosulfate and less bulky primary or secondary alkyl ammonium cations may be a favorable option to catalyze other nucleophilic addition reactions as well.

Acknowledgements

Y.A. gratefully acknowledges financial support from the Fulbright Visiting Scholar Program, and thanks Valerie Pitz for technical support. J.A. acknowledges financial support from the National Science Foundation (grant CHE-1265833). L.C.D. is grateful to FAPESP (2014/21930-9) and to CNPq for fellowships. The authors thank the Center for Computational Research (CCR) at the University at Buffalo for providing computational resources.

Keywords: catalysis · density functional calculations · ionic liquids · multisubstituted imidazole · solvation

[1] J. P. Hallett, T. Welton, *Chem. Rev.* **2011**, *111*, 3508–3579.
[2] Q. Bao, K. Qiao, D. Tomida, C. Yokoyama, *Catal. Commun.* **2008**, *9*, 1383–1388.
[3] P. A. Ganeshpure, G. George, J. Das, *J. Mol. Catal. A: Chem.* **2008**, *279*, 182–186.
[4] K. V. Wagh, B. M. Bhanage, *Green Chem.* **2015**, *17*, 4446–4451.
[5] Y. N. Shim, J. K. Lee, J. K. Im, D. K. Mukherjee, D. Q. Nguyen, M. Cheong, H. S. Kim, *Phys. Chem. Chem. Phys.* **2011**, *13*, 6197–6204.
[6] S. K. Mohamed, J. Simpson, A. A. Marzouk, A. H. Talybov, A. A. Abdelhamid, Y. A. Abdullayev, V. M. Abbasov, *Z. Naturforsch. B* **2015**, *70*, 809.
[7] S. Das Sharma, P. Hazarika, D. Konwar, *Tetrahedron Lett.* **2008**, *49*, 2216–2220.
[8] L.-M. Wang, Y.-H. Wang, H. Tian, Y.-F. Yao, J.-H. Shao, B. Liu, *J. Fluorine Chem.* **2006**, *127*, 1570–1573.
[9] L. Nagarapu, S. Apuri, S. Kantevari, *J. Mol. Catal. A: Chem.* **2007**, *266*, 104–108.
[10] A. R. Karimi, Z. Alimohammadi, J. Azizian, A. A. Mohammadi, M. R. Mohammadizadeh, *Catal. Commun.* **2006**, *7*, 728–732.
[11] M. Kidwai, P. Mothsra, V. Bansal, R. K. Somvanshi, A. S. Ethayathulla, S. Dey, T. P. Singh, *J. Mol. Catal. A: Chem.* **2007**, *265*, 177–182.
[12] A. R. Khosropour, *Ultrason. Sonochem.* **2008**, *15*, 659–664.
[13] a) Y. P. Yurenko, J. Novotný, M. P. Mitoraj, V. Sklenář, A. Michalak, R. Marek, *J. Chem. Theory Comput.* **2014**, *10*, 5353–5365; b) J. Dommerholt, O. van Rooijen, A. Borrmann, C. F. Guerra, F. M. Bickelhaupt, F. L. van Delft, *Nat. Commun.* **2014**, *5*, 5378; c) K. Muto, J. Yamaguchi, D. G. Musaev, K. Itami, *Nat. Commun.* **2015**, *6*, 7508; d) N. Menges, O. Sari, Y. Abdullayev, S. S. Erdem, M. Balci, *J. Org. Chem.* **2013**, *78*, 5184–5195.
[14] a) D. B. Nale, B. M. Bhanage, *Synlett* **2015**, *26*, 2835–2842; b) A. Maleki, Z. Alrezvani, S. Maleki, *Catal. Commun.* **2015**, *69*, 29–33; c) Y. Ran, M. Li, Z.-Z. Zhang, *Molecules* **2015**, *20*, 20286–20296; d) A. Ranjan, R. Yerande, P. B. Wakchaure, S. G. Yerande, D. H. Dethe, *Org. Lett.* **2014**, *16*, 5788–5791; e) S. S. K. Boominathan, C.-Y. Chen, P.-J. Huang, R.-J. Hou, J.-J. Wang, *New J. Chem.* **2015**, *39*, 6914–6918.
[15] N. C. Desai, A. R. Trivedi, H. C. Somani, K. A. Bhatt, *Chem. Biol. Drug Des.* **2015**, *86*, 370–377.
[16] A. Jallapally, D. Addla, P. Bagul, B. Sridhar, S. K. Banerjee, S. Kantevari, *Bioorg. Med. Chem.* **2015**, *23*, 3526–3533.
[17] O. Petrov, M. Gerova, K. Petrova, Y. Ivanova, *J. Heterocycl. Chem.* **2009**, *46*, 44–48.
[18] S. Johannsen, N. Megger, D. Böhme, R. K. O. Sigel, J. Müller, *Nat. Chem.* **2010**, *2*, 229–234.
[19] K. Hiraoka, T. Inoue, R. D. Taylor, T. Watanabe, N. Koshikawa, H. Yoda, K.-i. Shinohara, A. Takatori, H. Sugimoto, Y. Maru, T. Denda, K. Fujiwara, A. Balmain, T. Ozaki, T. Bando, H. Sugiyama, H. Nagase, *Nat. Commun.* **2015**, *6*, 6706.
[20] M. N. El-Haddad, A. S. Fouda, *J. Mol. Liq.* **2015**, *209*, 480–486.
[21] L. Li, Y. Fu, A. Manthiram, *Electrochem. Commun.* **2014**, *47*, 67–70.
[22] M. Ghorbani, S. Noura, M. Oftadeh, E. Gholami, M. A. Zolfigol, *RSC Adv.* **2015**, *5*, 55303–55312.

[23] Y. Zhao, D. G. Truhlar, *J. Chem. Phys.* **2006**, *125*, 194101.
[24] W. J. Hehre, R. Ditchfield, J. A. Pople, *J. Chem. Phys.* **1972**, *56*, 2257 – 2261.
[25] a) V. V. Chagovets, M. V. Kosevich, S. G. Stepanian, O. A. Boryak, V. S. Shelkovsky, V. V. Orlov, V. S. Leontiev, V. A. Pokrovskiy, L. Adamowicz, V. A. Karachevtsev, *J. Phys. Chem. C* **2012**, *116*, 20579 – 20590; b) M. Dračínský, R. Pohl, L. Slavětínská, J. Janků, M. Buděšínský, *Tetrahedron: Asymmetry* **2011**, *22*, 356 – 366.
[26] M. J. Frisch, G. W. Trucks, H. B. Schlegel, G. E. Scuseria, M. A. Robb, J. R. Cheeseman, G. Scalmani, V. Barone, B. Mennucci, G. A. Petersson, H. Nakatsuji, M. Caricato, X. Li, H. P. Hratchian, A. F. Izmaylov, J. Bloino, G. Zheng, J. L. Sonnenberg, M. Hada, M. Ehara, K. Toyota, R. Fukuda, J. Hasegawa, M. Ishida, T. Nakajima, Y. Honda, O. Kitao, H. Nakai, T. Vreven, J. A. Montgomery Jr., J. E. Peralta, F. Ogliaro, M. J. Bearpark, J. Heyd, E. N. Brothers, K. N. Kudin, V. N. Staroverov, R. Kobayashi, J. Normand, K. Raghavachari, A. P. Rendell, J. C. Burant, S. S. Iyengar, J. Tomasi, M. Cossi, N. Rega, N. J. Millam, M. Klene, J. E. Knox, J. B. Cross, V. Bakken, C. Adamo, J. Jaramillo, R. Gomperts, R. E. Stratmann, O. Yazyev, A. J. Austin, R. Cammi, C. Pomelli, J. W. Ochterski, R. L. Martin, K. Morokuma, V. G. Zakrzewski, G. A. Voth, P. Salvador, J. J. Dannenberg, S. Dapprich, A. D. Daniels, Ö. Farkas, J. B. Foresman, J. V. Ortiz, J. Cioslowski, D. J. Fox in *Gaussian 09*, *Vol. Gaussian 09*, *Revision D.01*, Gaussian, Inc., Wallingford, CT, USA, **2009**.
[27] A. V. Marenich, C. J. Cramer, D. G. Truhlar, *J. Phys. Chem. B* **2009**, *113*, 6378 – 6396.
[28] S. Kozuch, S. Shaik, *Acc. Chem. Res.* **2011**, *44*, 101 – 110.

Received: June 20, 2016
Published online on August 17, 2016

